

## A SUZAKU OBSERVATION OF MCG –2-58-22: CONSTRAINING THE GEOMETRY OF THE CIRCUMNUCLEAR MATERIAL

ELIZABETH RIVERS<sup>1</sup>, ALEX MARKOWITZ<sup>1</sup>, RICHARD ROTHSCHILD<sup>1</sup>

*Draft version September 28, 2018*

### ABSTRACT

We have analyzed a *Suzaku* long-look of the active galactic nucleus MCG –2-58-22, a type 1.5 Seyfert with very little X-ray absorption in the line of sight and prominent features arising from reflection off circumnuclear material: the Fe line and Compton reflection hump. We place tight constraints on the power law photon index ( $\Gamma=1.80\pm 0.02$ ), the Compton reflection strength ( $R=0.69\pm 0.05$ ), and the Fe K emission line energy centroid and width ( $E=6.40\pm 0.02$  keV,  $v_{\text{FWHM}} < 7100$  km s<sup>-1</sup>). We find no significant evidence for emission from strongly ionized Fe, nor for a strong, relativistically broadened Fe line, indicating that perhaps there is no radiatively efficient accretion disk very close in to the central black hole. In addition we test a new self-consistent physical model from Murphy & Yaqoob, the “MYTORUS” model, consisting of a donut-shaped torus of material surrounding the central illuminating source and producing both the Compton hump and the Fe K line emission. From the application of this model we find that the observed spectrum is consistent with a Compton-thick torus of material (column density  $N_{\text{H}}=3.6_{-0.8}^{+1.3} \times 10^{24}$  cm<sup>-2</sup>) lying outside of the line of sight to the nucleus, leaving it bare of X-ray absorption in excess of the Galactic column. We calculate that this material is sufficient to produce all of the Fe line flux without the need for any flux contribution from additional Compton-thin circumnuclear material.

*Subject headings:* Galaxies: active – X-rays: galaxies – Galaxies: Individual: MCG –2-58-22

### 1. INTRODUCTION

MCG –2-58-22 is an X-ray bright Seyfert 1.5 active galactic nucleus (AGN) located at a redshift of  $z = 0.04686$ . Past X-ray observations of this source performed with *EXOSAT*, *ASCA*, *XMM-Newton* and *BeppoSAX* have revealed the following spectral components in addition to the primary X-ray power law: a soft excess, Fe emission lines, and a Compton reflection hump. Importantly, there has been no evidence for X-ray absorption by gas along the line of sight in excess of the Galactic column, indicating that in the X-ray band this AGN is a “bare nucleus”. This combination makes MCG –2-58-22 an interesting target of study, since the lack of significant X-ray absorption provides a clean view of the nucleus with a relatively simple spectrum to model, while the presence of strong reflection components allows us to place constraints on the physical geometry of the circumnuclear material surrounding the AGN.

Ghosh & Soundararajaperumal (1992) analyzed *EXOSAT* data obtained in 1984 that revealed the highly variable soft excess below about 2 keV. They modeled this component with a steep power law in addition to their continuum power law. *ASCA* data covering 2.5–10 keV with good CCD resolution were analyzed by Weaver et al. (1995). They modeled the spectrum using a hard X-ray power law ( $\Gamma = 1.75 \pm 0.05$ ) with Galactic absorption and confirmed the need for a soft excess, as well as an Fe K $\alpha$  emission line which was unresolved. Weaver, Gelbord & Yaqoob (2001) analyzed two additional *ASCA* observations of MCG –2-58-22, tracking the Fe line flux over a time scale of years and showing large variation

in the flux of the underlying continuum. However large uncertainties precluded definitive conclusions about the variation of the Fe line parameters.

A more recent analysis by Bianchi et al. (2004) using simultaneous data from *XMM-Newton* and *BeppoSAX* covered a much broader energy range than previous observations (0.5–200 keV). Unfortunately only 7 ks of good EPIC-pn data were obtained for the source, providing only loose constraints in the Fe K bandpass (the Fe K $\alpha$  line was unresolved with  $\sigma < 340$  eV and an equivalent width, EW, of  $45_{-24}^{+85}$  eV). They were able to loosely constrain the Compton reflection hump with  $R = 0.4 \pm 0.3$  and  $\Gamma = 1.72_{-0.06}^{+0.08}$ .

In this paper we present an in-depth analysis of a single 140 ks long-look *Suzaku* observation of MCG –2-58-22. *Suzaku* is a Japanese observatory that provides broad-band X-ray spectra from  $\sim 0.5$  keV to above 500 keV with good energy resolution and effective area around 5–7 keV for detailed analysis of the Fe K complex (Mitsuda et al. 2007). Our goals for this observation were to study the Fe K emission, constrain the Compton hump, confirm the bare nucleus, and study the soft excess, all of which *Suzaku* is capable of doing well. This information can then be used to explore possibilities for the geometry of the circumnuclear material including the Fe line emitting gas and we improve upon parameter values in the literature for the Compton hump and Fe K emission lines. This paper is structured as follows: Section 2 details data reduction, Section 3 describes spectral fitting and analysis, and Section 4 contains a discussion of the results.

### 2. DATA REDUCTION AND ANALYSIS

*Suzaku* observed MCG –2-58-22 with the X-ray Imaging Spectrometer (XIS; Koyama et al. 2007) and the Hard

erivers@ucsd.edu

<sup>1</sup> University of California, San Diego, Center for Astrophysics and Space Sciences, 9500 Gilman Dr., La Jolla, CA 92093-0424, USA

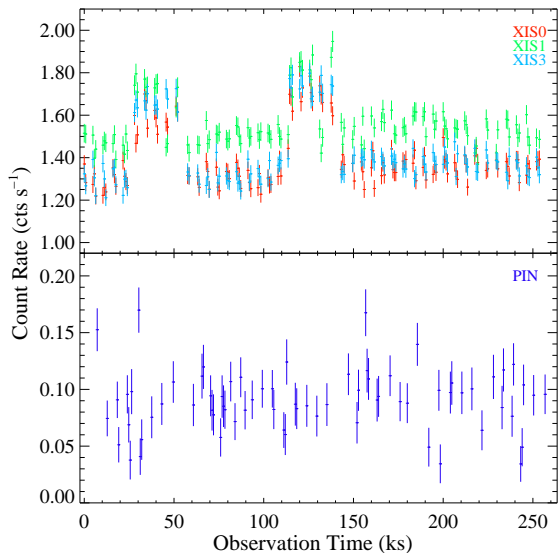


FIG. 1.— The lightcurve over the duration of the observation. Bins are 800 s. The XIS count rates are in the 2–10 keV range while the PIN count rates are in the 20–50 keV range. The increases in flux seen in the XIS around 30–50 ks and 110–140 ks are small (only about 20%) and flux-resolved spectroscopy did not reveal significant change in the shape of the spectrum during these episodes.

X-ray Detector (HXD; Takahashi et al. 2007) on 2009 November 27 beginning at 22:49 UT (Observation ID 704032010). Data were processed with version 2.4.12.27 of the *Suzaku* pipeline and typical screening criteria were applied (as per the *Suzaku* Data Reduction Guide<sup>2</sup>). All extractions were done using HEASOFT v.6.9.

### 2.1. XIS Reduction

The XIS is comprised of 3 CCD cameras<sup>3</sup> each placed in the focal plan of an X-ray Telescope module. Two of these (XIS0 and XIS3) are front-illuminated (FI), maximizing the effective area of the detectors in the Fe K bandpass, while the third (XIS1) is back-illuminated (BI), increasing its effective area in the soft X-ray band ( $\lesssim 2$  keV). Two corners of each XIS CCD are illuminated by an  $^{55}\text{Fe}$  calibration source, which can be used to calibrate the gain and test the spectral resolution of data taken using this instrument (see the *Suzaku* Data Reduction Guide for details).

After screening, the good exposure time per XIS was 138.9 ks. The XIS events data were in  $3\times 3$  and  $5\times 5$  editing modes which were cleaned and summed to create image files for each XIS. From these we extracted source and background lightcurves and spectra, using XISRMFGEN and XISSIMARFGEN to create the response matrix (RMF) and ancillary response (ARF) files. Data from the two front-illuminated CCDs were summed to create a single co-added FI spectrum after it was confirmed that the two spectra were consistent.

Data were ignored above 12 keV (10 keV for BI) where the effective area of the XIS begins to drop dramatically. Data were ignored below 1.0 keV (0.7 for BI which has a larger effective area at low energies) due to time-dependent calibration issues of the instrumental

O K edge at 0.5 keV, and between 1.5 and 2.4 keV due to large calibration uncertainties for the Si K complex and Au M edge arising from the detector mirror system. These issues are not fully understood at the time of this writing. Average 2–10 keV rates were  $1.410\pm 0.002$  and  $1.521\pm 0.003$  counts  $\text{s}^{-1}$  per XIS for FI and BI respectively. Figure 1 shows the XIS lightcurves for the duration of the observation.

Fitting the  $^{55}\text{Fe}$  calibration source spectra in XSPEC v.12.6.0 (Arnaud et al. 1996) with a model comprised of three Gaussian components (Mn  $K\alpha_1$ ,  $K\alpha_2$  and  $K\beta$ ) yielded the following results for the Mn  $K\alpha_1$  line energy (expected value of 5.899 keV): 5.886 keV (FI) and 5.890 keV (BI), showing that the energy calibration has a systematic uncertainty of  $\sim 10$  eV for both the FI and BI. Additionally, these lines had an average width of 30 eV, which we will take as instrumental broadening in excess of that modeled by the response matrix, and have subtracted this value in quadrature from all measured line widths.

### 2.2. PIN Reduction

The HXD gathered data with both its detectors, the PIN diodes and the GSO scintillators, however we did not use the GSO data because of the faintness of the source relative to the non-X-ray background in the GSO band. The HXD/PIN is a non-imaging instrument with a  $34'$  square (FWHM) field of view. The HXD instrument team provides non-X-ray background model event files using the calibrated GSO data for the particle background monitor (“background D” or “tuned background” with METHOD=LCFITDT). This yields instrument background estimates with  $\lesssim 1.5\%$  systematic uncertainty at the  $1\sigma$  level (Fukuzawa et al. 2009). As suggested in the *Suzaku* ABC Guide, the Cosmic X-ray Background was simulated in XSPEC v.12.6 using the form of Boldt (1987).

Net spectra were extracted and deadtime-corrected for a net exposure time of 98.0 ks. We excluded PIN data below 13 keV due to thermal noise and above 60 keV where the effective area of the detector falls significantly. The average 13–60 keV rate was  $0.202\pm 0.002$  counts  $\text{s}^{-1}$ . Figure 1 shows the PIN lightcurve for the duration of the observation.

## 3. SPECTRAL FITTING

All spectral fitting was done in XSPEC, utilizing solar abundances of Anders & Grevesse (1989) and cross-sections from Verner et al. (1996). All fits included absorption by the Galactic column with  $N_{\text{H Gal}}=2.70\times 10^{20}$   $\text{cm}^{-2}$  (Kalberla et al. 2005). Uncertainties are listed at the 90% confidence level ( $\Delta\chi^2 = 2.71$  for one interesting parameter).

### 3.1. The Fe K Bandpass

We began our analysis with a preliminary study focused on the Fe K bandpass. We used data from 4.5–8.5 keV from the FI spectrum only because of its excellent response and effective area in this energy range. We analyzed the Fe K complex, including the Fe  $K\alpha$  and  $K\beta$  lines and the Fe K edge, and investigated the possibility of emission from ionized Fe, namely Fe XXV or XXVI (the latter was reported by Bianchi et al. 2004 with a  $2\sigma$  detection).

<sup>2</sup> <http://heasarc.gsfc.nasa.gov/docs/suzaku/analysis/abc/abc.html>

<sup>3</sup> The fourth CCD camera, XIS2, is inoperative as of 2006 November. See the *Suzaku* ABC Guide for details.

TABLE 1  
 MODEL PARAMETERS

Model	$\Gamma$	$A^a$ ( $10^{-2}$ )	$E$ (keV)	$I^b$ ( $10^{-5}$ )	$\sigma$ (eV)	EW (eV)	$\tau$	$R$	$\Gamma_{\text{soft}}$	$A_{\text{soft}}^a$ ( $10^{-3}$ )	$\chi^2/\text{dof}$
Fe K Band	$1.68 \pm 0.05$	$1.15 \pm 0.08$	$6.40 \pm 0.02$	$2.8 \pm 0.6$	$60 \pm 30$	$50 \pm 10$	$0.05 \pm 0.02$				103/95
<b>Broadband 1</b>	$1.80 \pm 0.02$	$1.30 \pm 0.02$	$6.40 \pm 0.02$	$2.4 \pm 0.3$	$< 65$	$40 \pm 10$		$0.69 \pm 0.05$	$3.0 \pm 0.6$	$0.14^{+0.16}_{-0.07}$	604/464
Broadband 2	$1.83 \pm 0.01$	$1.37 \pm 0.01$	$6.40 \pm 0.02$	$2.4 \pm 0.3$	$< 60$	$41 \pm 5$		$0.76 \pm 0.07$	$k_B T$ (keV) $0.18 \pm 0.02$	$A_{\text{body}}^c$ $2.2 \pm 0.5$	611/464

NOTE. — Best fit parameters for models in the Fe K bandpass and broad band spectrum. “Fe K Band 1” is a model fit over the energy range 4.5–8 keV using only XIS1 (as described in Section 3.1) including the primary power law, Fe K $\alpha$  and K $\beta$  lines as Gaussians and the Fe K edge (“ZEDGE” in XSPEC). The Broadband models were fit over the energy range 0.7–50 keV using FI and BI XIS data as well as the PIN. Broadband 1 includes the continuum, Gaussian Fe emission lines, the Compton hump modeled with PEXRAV, and the soft excess modeled with a power law as described in Section 3.2. Broadband 2 differs from Broadband 1 in the use of a blackbody (“BBODY”) to model the soft excess. We adopt the parameters of the best fit to the Broadband 1 model for the discussion in Section 4.

<sup>a</sup> Power law normalization ( $\text{ph keV}^{-1} \text{cm}^{-2} \text{s}^{-1}$  at 1 keV)

<sup>b</sup> Fe K $\alpha$  line normalization ( $\text{ph cm}^{-2} \text{s}^{-1}$ )

<sup>c</sup> Blackbody normalization ( $10^{-5} \text{ph keV}^{-1} \text{cm}^{-2} \text{s}^{-1}$ )

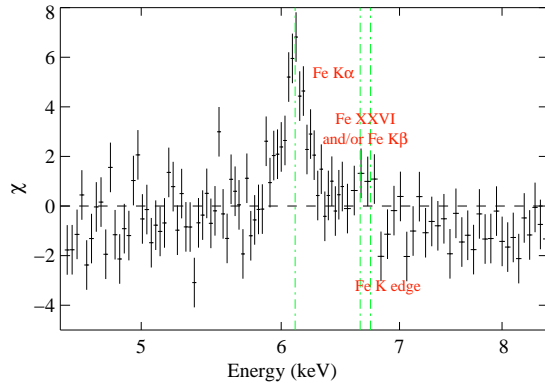


FIG. 2.— Data–model ratios to a simple power law fit for the Fe K band from 4.5–8.5 keV using the FI XIS data only. Dashed lines show expected locations (from left to right) of the energy centroids of the Fe K $\alpha$ , XXVI, and K $\beta$  lines. Note that these are the observed energies ( $z = 0.04686$ ).

As a first step we fit a simple power law with Galactic absorption. Model–data residuals for the simple power law are shown in Figure 2. This yielded a poor fit with  $\chi^2/\text{dof} = 322/100$  and obvious residuals around 6.4 keV (rest frame energy), the location of the Fe K $\alpha$  line. Fitting the line with a Gaussian component provided a much better fit with  $\chi^2/\text{dof} = 117/97$ . Visual inspection then revealed additional residuals around 7.1 keV (the location of the K $\beta$  line and Fe K edge).

We then added an edge component to model additional Fe K shell absorption in excess of the Galactic column and/or the Fe K edge associated with Compton reflection. We fixed the edge energy at 7.11 keV and left the optical depth ( $\tau$ ) free.  $\chi^2/\text{dof}$  dropped to 108/96, indicating a significant detection of the edge at a confidence level of  $\sim 99.4\%$  according to an  $F$ -test<sup>4</sup>.

Assuming an origin in neutral or lowly-ionized gas, an Fe K $\beta$  line should be present in addition to the Fe K $\alpha$  line. We added a Gaussian emission line with its energy

<sup>4</sup> Note that an  $F$ -test is inappropriate to perform in this case (see Protassov et al. 2002), however it can give a rough approximation of the significance.

centroid frozen at 7.056 keV (degeneracy with the Fe K edge at 7.11 keV and lack of sufficient line strength to provide good constraints led to our freezing the parameter at its expected value), its width tied to that of the K $\alpha$  line and its normalization left free. The fit improved, with  $\chi^2/\text{dof}$  dropping to 103/95 with a normalization of  $15 \pm 12\%$  of the K $\alpha$  normalization, consistent with that expected for cold/neutral gas. An  $F$ -test<sup>3</sup> indicates that this is a  $2\sigma$  detection at the  $\sim 96.4\%$  confidence level.

In some AGN, contributions to the total observed Fe K emission profile can arise from material which is ionized, either by collisional- or photo-ionization. Using XMM-Newton-EPIC data, Bianchi et al. (2004) found a degeneracy between the parameters of the K $\beta$  line and those from a possible Fe XXVI emission line. They reported a  $2\sigma$  detection of the Fe XXVI line when the K $\beta$  line was not included and with all the parameters of the line left free. When we allowed the energy of the K $\beta$  line to be free to vary we found an energy centroid of  $7.0 \pm 0.1$ , consistent with both the K $\beta$  and Fe XXVI line energies.  $\chi^2/\text{dof}$  was 102/95 (not a significant improvement) and the normalization was  $18 \pm 14\%$  of the K $\alpha$  normalization. Freezing the line energy at 6.966 keV, the weighted average of the Fe XXVI doublet, provided a fit virtually identical to the one presented above. Fitting both lines simultaneously with energies frozen at their expected values and widths tied to that of the K $\alpha$  line gave  $\chi^2/\text{dof} = 102/94$  with a normalization of  $13^{+18}_{-11}\%$  for Fe XXVI and an upper limit of 26% for K $\beta$  (both percentages are with respect to the K $\alpha$  normalization). We therefore cannot rule out the that the source may contain both emission lines and that we are simply unable to deblend them. For simplicity, in all further models described in this paper we have included only the K $\beta$  line with frozen or tied parameters.

We also tested for the presence of Fe XXV (using a Gaussian component with energy centroid fixed at 6.70 keV), however  $\chi^2/\text{dof}$  did not improve and only an upper limit to the normalization was obtained ( $\lesssim 6 \times 10^{-6} \text{ph cm}^{-2} \text{s}^{-1}$ ). Final parameters for the Fe K complex model fit including the K $\alpha$  line, Fe K edge and K $\beta$  line

are listed in Table 1 as the “Fe K Band” model, including the Fe  $K\alpha$  energy centroid ( $E$ ), intensity ( $I$ ), width ( $\sigma$ ), and EW.

We also tested the “DISKLINE” model for the emission lines in place of the more phenomenological Gaussian model. DISKLINE models the Doppler broadening of an emission line associated with the inner region of an accretion disk (Fabian et al. 1989). The diskline parameters were not well constrained, giving a very large inner radius ( $R_{\text{in}} \gtrsim 20 R_S$ , where  $R_S$  is the Schwarzschild radius) and a narrow profile. It did not improve the fit over a simple Gaussian. Next we tried the addition of a broad DISKLINE ( $R_{\text{in}}$  constrained to around  $3 R_S$  and energy fixed at 6.4 keV) to a narrow Gaussian line with energy and width fixed at the values found with the Gaussian fit (see Table 1). We obtained an upper limit to the DISKLINE normalization of  $\lesssim 2 \times 10^{-5} \text{ ph cm}^{-2} \text{ s}^{-1}$  and an EW of  $\lesssim 35 \text{ eV}$ . It is thus possible that a weak broad line exists in this source and that we are simply unable to detect it; however combining the weakness of this feature with the lack of ionized emission indicates that most if not all of the Fe line flux comes from material that is not close in to the central black hole.

It is possible that such a weak broad line would be degenerate with the Compton shoulder, a feature which could arise if there is a significant amount of Compton-thick material. Additionally, by visual inspection we see a shallow shelf-like shape in the residuals on the low-energy side of the emission line when  $\sigma$  is set to  $\lesssim 30 \text{ eV}$ . We tested this by modeling a moderately broad Gaussian in addition to the narrow Fe  $K\alpha$  line in the “Fe K Band 2” model with an energy centroid fixed at 6.34 keV (Matt 2002). This resulted in an improvement in  $\chi^2/\text{dof}$  of only 2/1, which is not a significant detection but indicates that the Compton shoulder should be tested for in future observations.

### 3.2. Broadband Fitting

Next we fit the broadband spectrum of MCG -2-58-22 covering the range from 0.7–60 keV. We used the XIS FI, XIS BI, and PIN spectra. We included an instrumental cross-normalization constant in our fits with the PIN constant set to 1.16 (this is the expected value for XIS-nominal pointing and leaving the parameter free caused degeneracy with the Compton reflection component in our models) and the BI constant left free relative to the FI spectrum (values were typically around  $\sim 1.05$ ). The broadband data are shown in Figure 3a. Figure 3b shows residuals to a simple power law fit in which we can clearly see the need for modeling the Fe K complex, Compton reflection peaking around 20–30 keV, and a soft excess below  $\sim 1 \text{ keV}$ .

We began by modeling the soft excess with a simple power law in addition to the continuum power law and modeling the Compton reflection hump using PEXRAV (Magdziarz & Zdziarski, 1995) which assumes a disk-like geometry for the reflecting material and where the value of  $R$  is the proportion of the primary power law that is reflected off Compton-thick material. Best fit parameters for this model are listed under “Broadband 1” in Table 1 and data-model residuals are shown in Figure 3c. We did not find the need for additional cold absorption with an upper limit to the column density of  $2.5 \times 10^{20} \text{ cm}^{-2}$

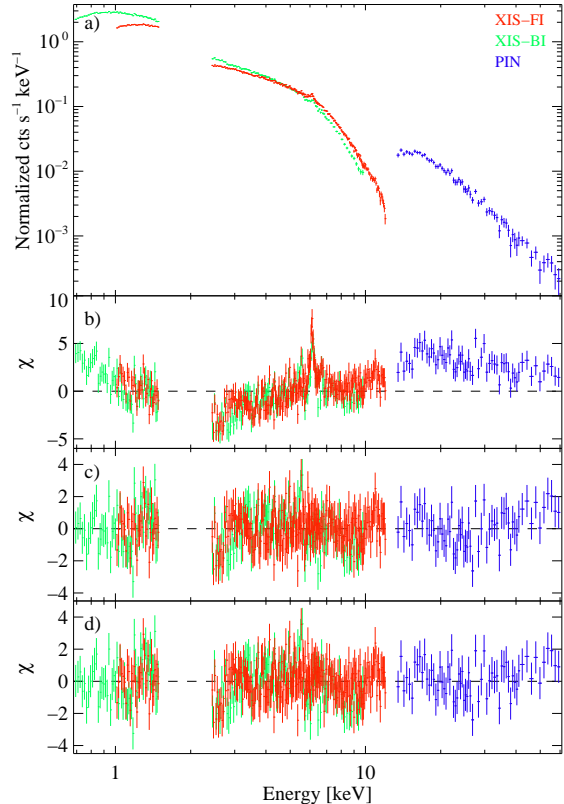


FIG. 3.— Spectral fitting for MCG -2-58-22 from 0.7–50 keV. Panel a) shows the data from the XIS FI and BI, and the PIN. Panel b) shows the data-model residuals for a simple absorbed power law. Panel c) shows the data-model residuals for our best-fit disk/slab geometry model including the iron lines, soft excess and Compton hump in addition to the continuum. Panel d) shows the data-model residuals for our best fit torus geometry model utilizing MYTORUS. It is obvious that the fits shown in panels c) and d) are virtually identical though the modelling is quite different.

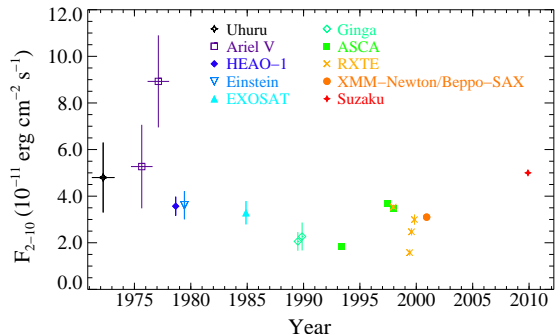


FIG. 4.— Historical values for the 2–10 keV flux. From left to right this source has been observed by *Uhuru* (Cooke et al. 1978), *Ariel-V* (Marshall, Warwick & Pounds 1981), *HEAO-1* (Griffiths et al. 1979), *Einstein* (Turner et al. 1991), *EXOSAT* (Ghosh & Soundararajaperumal 1992), *Ginga* (Nandra & Pounds 1994), *ASCA* (Weaver et al. 1995), *RXTE*, simultaneously by *XMM-Newton/BeppoSAX* (Bianchi et al. 2004), and most recently by *Suzaku* (this paper).

in excess of the Galactic. We also tested for the presence of warm absorption using an XSTAR table but found it unnecessary for a good fit. The Compton reflection hump and Fe K edge were well fit by the PEXRAV model and Fe line parameters were very similar to those found from narrow band fitting, including the upper limit to

a relativistically broadened DISKLINE component. The observed 2–10 keV flux was  $F_{2-10}=5.0 \pm 0.1 \times 10^{-11}$  ergs cm $^{-2}$  s $^{-1}$  and the intrinsic luminosity, calculated using the cosmology-corrected luminosity distance given by the NASA/IPAC Extragalactic Database<sup>5</sup>, and correcting for Galactic absorption was  $L_{2-10}=2.30 \pm 0.05 \times 10^{44}$  ergs s $^{-1}$ . Figure 4 shows historical values of the flux of this source in the 2–10 keV range.

We also tried a (phenomenological) blackbody emission component to model the soft excess. Parameters are listed in Table 1 under “Broadband 2”. Both the blackbody and power law models fit the data reasonably well, but in both cases parameters were difficult to constrain due to calibration issues with the O K edge below about 1 keV. For simplicity we adopt Broadband 1 as our best-fit model for the discussion in Section 4.

Bianchi et al. (2004) tested for high energy cut offs in their sample finding model-dependent values of  $E_c \sim 200$  keV with error bars of 50–800 keV. Extending up to only 60 keV, our data are not highly sensitive to a high energy cut off or rollover. Utilizing the “CUTOFFPL” model in XSPEC we found a lower limit to the rollover energy of 500 keV.

### 3.3. Applying a Self-Consistent Model

As our knowledge of AGN improves, so too should the sophistication of our modeling. Self-consistent models should be able to simultaneously model absorption and reflection by circumnuclear material, combining the Fe line, Compton reflection hump and column density along the line of sight. We have applied the model “MYTORUS” (Murphy & Yaqoob 2009) to our spectrum of MCG–2-58-22 which assumes the circumnuclear material is a donut shape of uniform density and includes all three of the components listed above.

The MYTORUS model was derived from Monte Carlo simulations of a dusty torus of uniform density surrounding an illuminating supermassive black hole. Relevant parameters to the model include the following:  $N_{\text{HTOR}}$ , the column density of the material in the torus (not necessarily in the line of sight);  $\theta_{\text{incl}}$ , the inclination angle of the torus, with 0° corresponding to a face-on view, 90° corresponding to edge-on, and with the torus intersecting the line of sight for angles larger than 60° (the assumed half-opening angle); the photon index ( $\Gamma$ ) and the normalization ( $A_{\text{PL}}$ ) of the illuminating power law; the width ( $\sigma$ ) of the Fe K $\alpha$  line (the material is assumed to be cold and the energy is not a free parameter); and with additional parameters  $A_{\text{S}}$  and  $A_{\text{L}}$ , the normalization factors of the Compton hump and Fe line respectively, to be used when the amount observed for either is significantly different from that expected by the model due to differences in covering factors, abundances, etc., from those assumed. We also included an additional power law for the soft excess.

We found a reasonably good fit ( $\chi^2/\text{dof} = 623/465$ , very similar to the broadband fit  $\chi^2$  values given in Table 1) with  $\theta_{\text{incl}}$  fixed at 30° (there was no significant improvement in fit with this parameter free). Since there is no extra absorption in MCG–2-58-22, the value obtained for  $N_{\text{HTOR}}$  is driven primarily by the strength of

the Compton reflection hump and Fe line. When  $A_{\text{L}}$  was free to vary there was an improvement in  $\chi^2$  of 9 for 1 less degree of freedom. We obtained a value for  $A_{\text{L}}$  of  $0.75 \pm 0.14$ , that is the amount of material creating the Fe line was about 75% of that creating the Compton hump, possibly due to an underabundance of Fe or geometrical effects not taken into account by the model (it should also be noted that the upper uncertainty on  $A_{\text{L}}$  is consistent with the lower uncertainty on  $N_{\text{HTOR}}$ ). Testing for an additional relativistically broadened Fe line yielded an upper limit to the normalization of  $\lesssim 1.5 \times 10^{-5}$  ph cm $^{-2}$  s $^{-1}$  and an EW of  $\lesssim 30$  eV. Our best fit parameters are listed in Table 2 and data–model residuals are shown in Figure 3d.

## 4. DISCUSSION AND CONCLUSIONS

### 4.1. The Fe K Complex

Focusing on the Fe K band we found the need for both Fe K $\alpha$  and K $\beta$  emission lines as well as an Fe K shell absorption edge (in broadband fits this edge was modeled sufficiently by the edge associated with the Compton reflection hump in both PEXRAV and MYTORUS). From the value of the emission line width found in our best-fit broadband model we calculated the velocity full width at half maximum ( $v_{\text{FWHM}}$ ) of the emitting material to be  $< 7100$  km s $^{-1}$ . This is consistent with values obtained for the optical H $\beta$  broad emission line of around 6400–8500 km s $^{-1}$  (Osterbrock 1977; Kollatschny & Dietrich 2006; Winter et al. 2010) and is a significant improvement on previous upper limits set by Weaver et al. (1991) and Bianchi et al. (2004) of  $\lesssim 30,000$  km s $^{-1}$ . Using a black hole mass estimated from optical luminosity and line widths to have a value of  $10^{8.4} M_{\odot}$  (Bian & Zhao 2003; Winter et al. 2010) and assuming Keplerian motion of the emitting material, we estimated the radius of the emitting region to be  $\gtrsim 45$  lt-days or roughly  $1200 R_{\text{S}}$ .

We also tested for a broad line and Compton shoulder. According to de la Calle Pérez et al. (2010), roughly  $\gtrsim 1.5 \times 10^5$  counts in the 2–10 keV band at CCD resolution provide good enough statistical quality to significantly detect a broad line. In the combined FI XIS we have  $\sim 4 \times 10^5$  counts, and our upper limit on the EW of a broad line places us in the lower part of the EW range of detected broad lines in the FEROS sample of Seyferts observed with *XMM-Newton*, wherein significant detections of broad lines with EW’s in the range of 50–250 eV were reported. We conclude that a very strong broad line ( $\gtrsim 50$  eV) does not exist in MCG–2-58-22 or else our observation would have been sufficient to significantly detect it; if there does exist a broad line in this source, then it must be very weak.

We would expect to see a Compton shoulder given the presence of Compton-thick material, however we did not obtain a significant detection. It should also be noted that the Compton shoulder is included in the MYTORUS model automatically, based on the strength of the Fe line and the column density of the torus.

### 4.2. Reflection and Geometry of the Circumnuclear Material

This source also shows a very prominent Compton hump around 20–30 keV (see Figure 3b). This feature, arising from Compton scattering of high energy photons

<sup>5</sup> <http://nedwww.ipac.caltech.edu/>

TABLE 2  
MODEL PARAMETERS FOR MYTORUS

$\Gamma$	$A_{\text{PL}}^1$ ( $10^{-2}$ )	$N_{\text{H Tor}}$ ( $10^{24} \text{ cm}^{-2}$ )	$A_{\text{L}}$	$\sigma$ (eV)	$\Gamma_{\text{soft}}$	$A_{\text{soft}}^1$ ( $10^{-3}$ )	$\chi^2/\text{dof}$
1.70±0.01	1.13±0.03	3.6 $^{+1.3}_{-0.8}$	0.75 ±0.14	<70	2.5±0.3	0.4 $^{+0.4}_{-0.2}$	623/465

NOTE. — Best fit parameters for the self-consistent MYTORUS model with  $\theta_{\text{incl}}$  fixed at  $30^\circ$  as discussed in Section 3.3.

<sup>1</sup> Power law normalization (ph keV $^{-1} \text{ cm}^{-2} \text{ s}^{-1}$  at 1 keV)

off Compton thick material in the vicinity of the black hole, is often associated with the Fe line emission seen in AGN, since the same Compton thick material that produces the Compton hump also produces Fe K emission. By knowing the (model-dependent) relationship between the strength of the Compton hump ( $R$ ) and the expected Fe line EW, we can test if Compton thick gas is capable of accounting for the entire observed Fe line flux.

Based on calculations done by George and Fabian (1991) for a disk geometry, we found that the expected Fe line EW for our value of  $R$  (assuming an inclination of  $30^\circ$  and solar abundances) is  $\sim 80 \pm 6$  eV. In our broadband fits we see a considerably milder Fe line flux with an EW closer to 40 eV, about half of the expected value. We found a similar, though less robust result using MYTORUS, with  $A_{\text{L}} = 0.75 \pm 14$  and  $\text{EW} = 47 \pm 6$  eV (calculated from the flux of the line) which assumes a “donut-like” geometry, in this case a Compton-thick torus out of the line of sight to the nucleus. In both cases we have found a lower than expected Fe line EW, possibly due to an underabundance of Fe. This makes it unlikely that there is significant contribution to the Fe line flux from Compton thin material in the vicinity of the black hole. This is in contrast to many Seyferts; for example the sample of Rivers et al. (2011), which utilized the PEXRAV disk reflection model, found that on average only  $\sim 30\%$  of the Fe line flux in Seyferts is associated with the Compton reflection component, implying the presence of substantial amounts of Compton-thin material and/or supersolar abundances of Fe. However other samples of Seyferts observed with *BeppoSAX* and *XMM-Newton* (Perola et al. 2002; Bianchi et al. 2004) were shown to have values of EW and  $R$  consistent with the Fe line and reflection hump arising in the same material assuming a slab (disk) geometry and a torus geometry respectively. In all cases uncertainties have been quite large and further investigation is warranted.

#### 4.3. Optical Obscuration and X-ray Absorption

We have confirmed that MCG –2-58-22 is unabsorbed in the X-ray band, a fact which is interesting considering its optical classification as a Seyfert 1.5 (Winkler 1992; Winter et al. 2010). Standard unification schemes would suggest that it should have less obscuration in the X-ray band than a typical Seyfert 2 but more than a typical Seyfert 1. However this is not the case, as we have obtained a very low upper limit on column density in excess of the Galactic. The question then, is whether there is material in the line of sight to the optical emission from this AGN that is *not* in the line of sight to the X-ray emitting region.

Optical reddening from dust can be characterized by

the visual extinction ( $A_{\text{v}}$ ), which we calculated from the flux ratio of  $\text{H}\alpha$  to  $\text{H}\beta$ , using the observed values of Winkler (1992) and assuming the intrinsic value of the Balmer decrement to be 2.87 (Osterbrock 1989). We found  $A_{\text{v}} \sim 1.97$  mag. From this value we calculated the inferred column density of gas using the relation of Predehl & Schmitt (1995),  $N_{\text{H}} = (1.79 \times 10^{21} \text{ cm}^{-2}) A_{\text{v}}$ , and assuming the Galactic gas/dust ratio holds. We inferred a column density of  $\sim 3.55 \times 10^{21} \text{ cm}^{-2}$ , an order of magnitude higher than our upper limit on the observed X-ray absorption column (in excess of the Galactic) of  $2.5 \times 10^{20} \text{ cm}^{-2}$ . Therefore, assuming the X-ray absorbing gas and optical absorbing dust track each other, the dust obscuring the optical broad line region is most likely *not* in the line of sight to the X-ray emitting regions. The inferred column density is also far too low to be associated with the dusty torus out of the line of sight which must be Compton-thick in order to produce the strong reflection component that we see (MYTORUS gives a column density of  $3.6^{+1.6}_{-0.9} \times 10^{24} \text{ cm}^{-2}$ ).

Since the X-ray emitting region is theorized to be very close in to the central black hole, it seems unlikely that this dust is in the form of an extended cloud in the host galaxy lying far (kiloparsecs) from the black hole that just happens to have a hole in the right place to produce a bare nucleus in the X-rays. The dust must be distinct, however, from the Compton-thick torus, given the low inferred column density and evidence that we are viewing the AGN more or less face on. One possible explanation for this set of constraints is that there is clumpy material in the line of sight and it happens that none of the clumps are obscuring the X-ray emitting region (see, e.g., Nenkova et al. 2008), only the optical broad line region. If future X-ray monitoring discovers a sudden, short-term increase in  $N_{\text{H}}$ , this scenario may be supported. Another explanation is that the material is commensurate with the broad line region, thus obscuring only this region.

#### 4.4. Conclusions

*Suzaku* is an ideal tool for studying AGN, providing us with a detailed look at many crucial components of AGN spectra. We confirmed that MCG –2-58-22 is extremely unabsorbed in the X-ray band (an upper limit of  $2.5 \times 10^{20} \text{ cm}^{-2}$  in excess of the Galactic column), despite significant reddening seen in the optical band. These results led us to conclude that while no absorbers are in the line of sight to the central region of the AGN, it is possible that clumps of material may be obscuring lines of sight to the region(s) where the optical line emission is produced.

With the excellent resolution of the XIS CCDs around

$\sim 5\text{--}7$  keV we were able to accurately study the Fe K complex. We found a narrow ( $v_{\text{FWHM}} < 7100 \text{ km s}^{-1}$ ) Fe  $K\alpha$  emission line and were able to constrain the location of the emitting material to much farther out than has been done with previous observations. We detected no significant broad Fe line as we would expect to see from the inner portions of a radiatively efficient accretion disk. Since we have such a clean line of sight to the nucleus, this region cannot be simply obscured or out of our line of sight, implying that the inner disk may be truncated or radiatively inefficient. From our limits on the Fe line  $v_{\text{FWHM}}$  we have calculated a minimum inner radius of  $\gtrsim 1200 R_{\text{S}}$ . We were also able to associate the Fe emission complex with the Compton reflection component in our models. Our results indicate that both components likely arise in the same Compton-thick material without any contribution from additional Compton-thin circumnuclear material. Assuming a disk/slab geometry (the PEXRAV model in XSPEC) for the Compton-thick material gave a reflection strength  $R=0.69\pm 0.05$  with a photon index of  $\Gamma=1.80\pm 0.02$ .

We successfully applied the new MYTORUS model for Compton reflection, which assumes that the reflecting material is in the form of a torus of uniform density rather than in the form of a flat disk, as has typically been done with more established models such as PEXRAV. Our results gave a photon index of  $\Gamma=1.70\pm 0.01$  with a column density of  $N_{\text{H}}=3.6^{+1.3}_{-0.8} \times 10^{24} \text{ cm}^{-2}$  for the torus. Additionally we found a lower than expected normalization for the Fe line, possibly due to subsolar abundances of Fe with  $Z_{\text{Fe}}=0.75\pm 0.14$ .

This research has made use of data obtained from the *Suzaku* satellite, a collaborative mission between the space agencies of Japan (JAXA) and the USA (NASA). This work has made use of HEASARC online services, supported by NASA/GSFC, and the NASA/IPAC Extragalactic Database, operated by JPL/California Institute of Technology under contract with NASA. This research was supported by NASA contract NAS5-30720, and NASA grants NNX08AD72G and NNX10AH87G.

## REFERENCES

- Anders, E. & Grevesse, N., 1989, *Geochimica et Cosmochimica Acta* 53, 197  
 Arnaud, K. 1996, in *Astronomical Data Analysis Software and Systems*, Jacoby, G., Barnes, J., eds., ASP Conf. Series Vol. 101, p.17  
 Bian, W. & Zhao, Y., 2003, *MNRAS*, 343, 164  
 Bianchi, S., Matt, G., Balestra, I., Guainazzi, M., & Perola, G.C., 2004, *A&A*, 422, 65  
 Boldt, E., 1987, *Proc. IAU Symp.* 124, *Observational Cosmology* (Dordrecht: Reidel), 611  
 Cooke, B.A., et al. 1978, *MNRAS*, 182, 489  
 de la Calle Pérez, I. et al. 2010, *A&A*, 524, 50  
 Fabian, A.C., Rees, M.J., Stella, L., White, N.E., 1989, *MNRAS*, 238, 729  
 Fukazawa, Y., et al. 2009, *PASJ*, 61, 17  
 Ghosh, K.K. & Soundararajaperumal, S., 1992, *ApJ*, 398, 501  
 George, I.M. & Fabian, A.C., 1991, *MNRAS*, 249, 352  
 Griffiths, R.E., Briel, U., Schwartz, D.A., Schwarz, J., Doxsey, R.E., & Johnston, M.D., 1979, *MNRAS*, 188, 813  
 Kalberla, P.M.W. et al. 2005, *A&A*, 440, 775  
 Koyama, K. et al. 2007, *PASJ*, 59, 23  
 Kollatschny, M.Z. & Dietrich, M., *A&A*, 454, 459  
 Marshall, N., Warwick, R.S., & Pounds, K.A., 1981, *MNRAS*, 194, 987  
 Matt, G., 2002, *MNRAS*, 337, 147  
 Magdziarz, P. & Zdziarski, A., 1995, *MNRAS*, 273, 837  
 Mitsuda, K., et al. 2007, *PASJ*, 59, 1  
 Murphy, K. D. & Yaqoob, T., 2009, *MNRAS*, 397, 1549  
 Nenkova, M. et al. 2008, *ApJ*, 685, 160  
 Osterbrock, D. E., 1977, *ApJ*, 215, 733  
 Osterbrock, D. E., 1989, *Astrophysics of Gaseous Nebulae and Active Galactic Nuclei*, (Mill Valley, CA: Univ. Science Books)  
 Predehl, P. & Schmitt, J.H.M.M., 1995, *A&A*, 293, 889  
 Protassov, R., van Dyk, D. A., Connors, A., Kashyap, V. L., & Siemiginowska, A. 2002, *ApJ*, 571, 545  
 Rivers, E., Markowitz, A., & Rothschild, R., 2011, *ApJS*, 193, 3  
 Takahashi, T., et al. 2007, *PASJ*, 59, 35  
 Turner, T.J., Weaver, K.A., Mushotzky, R.F., Holt, S.S., & Madejski, G.M., 1991, *ApJ*, 381, 85  
 Verner, D. A., Ferland, G. J., Korista, K. T., & Yakovlev, D. G. 1996, *ApJS*, 465, 487  
 Weaver, K.A., Gelbord, J. & Yaqoob, T., 2001, *ApJ*, 550, 261  
 Weaver, K.A., Nousek, J., Yaqoob, T., Hayashida, K., & Murakami, S. 1995, *ApJ*, 451, 147  
 Wilms, J., Allen, A., & McCray, M. 2000, *ApJ*, 542, 914  
 Winkler, H., 1992, *MNRAS*, 257, 677  
 Winter, L.M., Lewis, K.T., Koss, M., Veilleux, S., Keeney, B., & Mushotzky, R.R., 2010, *ApJ*, 710, 503